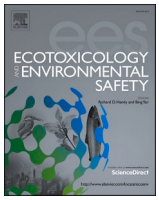
Ecotoxicology and Environmental Safety 287 (2024) 117307



Contents lists available at ScienceDirect

Ecotoxicology and Environmental Safety

journal homepage: www.elsevier.com/locate/ecoenv





Selenium protects mouse spermatogonia against ivermectin-induced apoptosis by alleviating endoplasmic reticulum stress *in vitro*

Daniel Chavez Varias, Sung-Hwan Moon, Seung Hee Shin, Buom-Yong Ryu *

Department of Animal Science and Technology, Chung-Ang University, Anseong-Si, Gyeonggi-Do 17546, Republic of Korea

ARTICLE INFO

Editor: Bing Yan

Keywords:
Ivermectin
Selenium
Redox Imbalance-associated Endoplasmic Reticulum (ER) Stress
Male infertility

ABSTRACT

Ivermectin (IVM) is a widely used anthelmintic in human and veterinary medicine. However, the increasing use of IVM raises concerns about its potential harm against non-targeted organisms. This study demonstrates a novel mechanism where IVM triggers apoptosis via endoplasmic reticulum (ER) stress in GC-1 spg *in vitro*. The inhibitory effects of selenium (Se) against the toxicological mechanism were also explored. IVM dose-dependently induces oxidative stress, dysregulated Ca^{2+} levels, and intracellular protein aggregation. Increased mitochondria-associated ER membrane (MAM) activity through Glucose-regulated Protein 75 (Grp75) overloads the mitochondria with Ca^{2+}, causing mitochondrial dysfunction. These simultaneous stressors lead to unfolded protein response and apoptosis. Se reverses all these subcellular events by promoting the expression of selenoprotein-encoding genes to maintain the ER and redox homeostasis. The testis-enriched Glutathione Peroxidase 4 (*Gpx4*) and the testis-specific Selenoprotein V (*Selenov*) are only upregulated in the IVM and Se co-treatment group, suggesting their potential role in stress response. These findings confirm that toxic doses of IVM lead to programmed cell death in type B spermatogonia through redox imbalance-associated ER stress. This study provides valuable insights into refining male reproductive toxicity evaluation, targeting of ER stress to protect male germ cells, and maintaining male fertility from IVM-induced toxicity.

1. Introduction

Ivermectin (IVM) is an anthelmintic under the avermectin class of macrocyclic lactones used in both human and veterinary medicine. It combats the four main soil-transmitted helminth infections: ascariasis, hookworm infections, trichuriasis, and strongyloidiasis (Boussinesq, 2018; Laman et al., 2022; Specht and Keiser, 2023). IVM is usually administered as a racemic mixture of two isomers, B1a and B1b (Fig. 1A) (Choudhury et al., 2021) and has a global market value exceeding one billion USD annually (Salman et al., 2022). It recently gained significant attention during the COVID-19 pandemic, and may continue to be seen as a 'wonder drug' beyond its anthelmintic use (Chaccour and Rabinovich, 2019; Foy et al., 2019; Sulik et al., 2023). However, its increasing use raises concerns about its safety and ecotoxicological impacts.

Recent studies found how contamination of avermectins poses extreme toxicity for aquatic life (Gan et al., 2024; Huang et al., 2019). The margin of safety of IVM concentrations between its target and non-target organisms is narrow (Novelli et al., 2016), and IVM's high-dose adverse effects on rats, mice, and companion animals have been reported (Bai and Ogbourne, 2016). However, there is a lack of comprehensive toxicity evaluation of avermectin compounds except abamectin against non-targeted species. The currently suggested guidelines of Environmental Risk Assessment of Pharmaceuticals may

Abbreviations: AV, Annexin V; APC, allophycocyanin; Atf4, activating transcription factor 4; Bcl-2, B-cell lymphoma 2; Chop, C/EBP homologous protein; CLD, compact letter display; DCFDA, dichlorodihydrofluorescein diacetate; DMEM, dulbecco's modified eagle medium; ER, endoplasmic reticulum; FBS, fetal bovine serum; Fas, Fas receptor; Gapdh, Glyceraldehyde-3-phosphate dehydrogenase; GluClR, glutamate-gated chloride channel receptor; Gpx1, glutathione peroxidase 1; Gpx4, glutathione peroxidase 4; Grp75, glucose-regulated protein 75; Grp78, glucose-regulated protein 78; Herpud1, homocysteine-inducible, endoplasmic reticulum stress-inducible, ubiquitin-like domain member 1; IVM, ivermectin; PI, propidium iodide; PVDF, polyvinylidene difluoride; qRT-PCR, quantitative reverse transcription-polymerase chain reaction; ROS, reactive oxygen species; Se, selenium; Selenoh, selenoprotein H; Selenom, selenoprotein m; Selenov, selenoprotein V; MAM, mitochondria-associated endoplasmic reticulum membrane; TBEA, trypan blue exclusion assay; ThT, thioflavin T; Tnfα, tumor necrosis factor alpha; UPR, unfolded protein response.

* Corresponding author.
E-mail address: byryu@cau.ac.kr (B.-Y. Ryu).

https://doi.org/10.1016/j.ecoenv.2024.117307
Received 18 June 2024; Received in revised form 21 October 2024; Accepted 5 November 2024
Available online 8 November 2024
0147-6513/© 2024 The Authors. Published by Elsevier Inc. This is an open access article under the CC BY-NC license (http://creativecommons.org/licenses/by-nc/4.0/).

not account for the use of IVM in areas with high helminth transmission or agricultural practices, resulting in underestimated environmental concentrations (Mesa et al., 2020; Tsheten et al., 2024).

The mechanism of IVM toxicity also remains unclear. Its anthelmintic action relies on activating the glutamate-gated chloride channel receptor (GluClR) in the helminth's nervous system. However, GluClR is protected by the blood-brain barrier in non-aquatic vertebrates (Atif et al., 2019). This suggests that IVM's toxicological mechanisms in vertebrates are yet to be fully understood. Mechanistic and dose-dependent studies on IVM are crucial to assess its ecological impact and refine toxicity evaluation tools.

Spermatogenesis is the intricate process of developing functional male gametes in the testis. It relies not only on cell differentiation but also equational and reductional division of spermatogonia to pass genetic material to offspring (Whelan et al., 2022). Several studies have highlighted IVM's potential to impair testicular function and reduce fertility, as shown by histopathological findings in male animal models. These studies report increased oxidative stress, apoptosis, necrosis, and defects in reproductive development (Ahmed et al., 2020; Cordeiro et al., 2018; EL-Maddawy and Abd El Naby, 2018; El-Shobokshy et al., 2023). However, the precise molecular mechanism behind IVM-induced loss of spermatogonia remains unclear.

The endoplasmic reticulum (ER) is the most important organelle for proper folding of proteins, calcium storage, and lipid synthesis. Redox homeostasis within the ER is critical because disulfide bonds during protein folding directly depends on the degree of oxidation. Misfolded proteins accumulate when disulfide bonds erroneously increase with reactive oxygen species (ROS), the byproducts of this chemical reaction. Additionally, oxidative stress may trigger calcium ion (Ca^{2+}) release from the ER into the cytosol (Bhattarai et al., 2021; Z. Zhang et al., 2019). Through the Ip3r1-Grp75-Vdac1 axis, excess Ca^{2+} may also mobilize to the mitochondria, causing mitochondrial dysfunction and contributing to increased ROS and cytosolic Ca^{2+} via the mitochondrial permeability transition pore (mPTP) (Li et al., 2022; Ma et al., 2023; Tiwary et al., 2021; T. Zhang et al., 2023; Y. Zhang et al., 2023). The additive effects of these stressors may ultimately lead to programmed cell death.

The spermatogonia strictly require a homeostatic ER for accurate post-translational modifications in proteins essential for spermatogenesis. Spermatogonia development is tightly regulated especially in protein synthesis because they rapidly divide and differentiate in multiple steps to become fertile sperm (Liu et al., 2014; C. Xu et al., 2021; Zhang et al., 2024). Dysfunctional ER in spermatogonia leads to ER stress, cell death, and defective sperm development and maturation. However, IVM's ability to induce ER stress is unconfirmed. Testicular function is also highly sensitive to changes in redox balance, and oxidative stress commonly couples with testicular pathogenesis. Many studies have shown IVM's ability to generate ROS, leading to cell death (Chen et al., 2020; Draganov et al., 2021; Jawad and Richardson, 2023; D. E. Lee et al., 2022; Tung et al., 2022; N. Xu et al., 2021; P. Zhang et al., 2019;

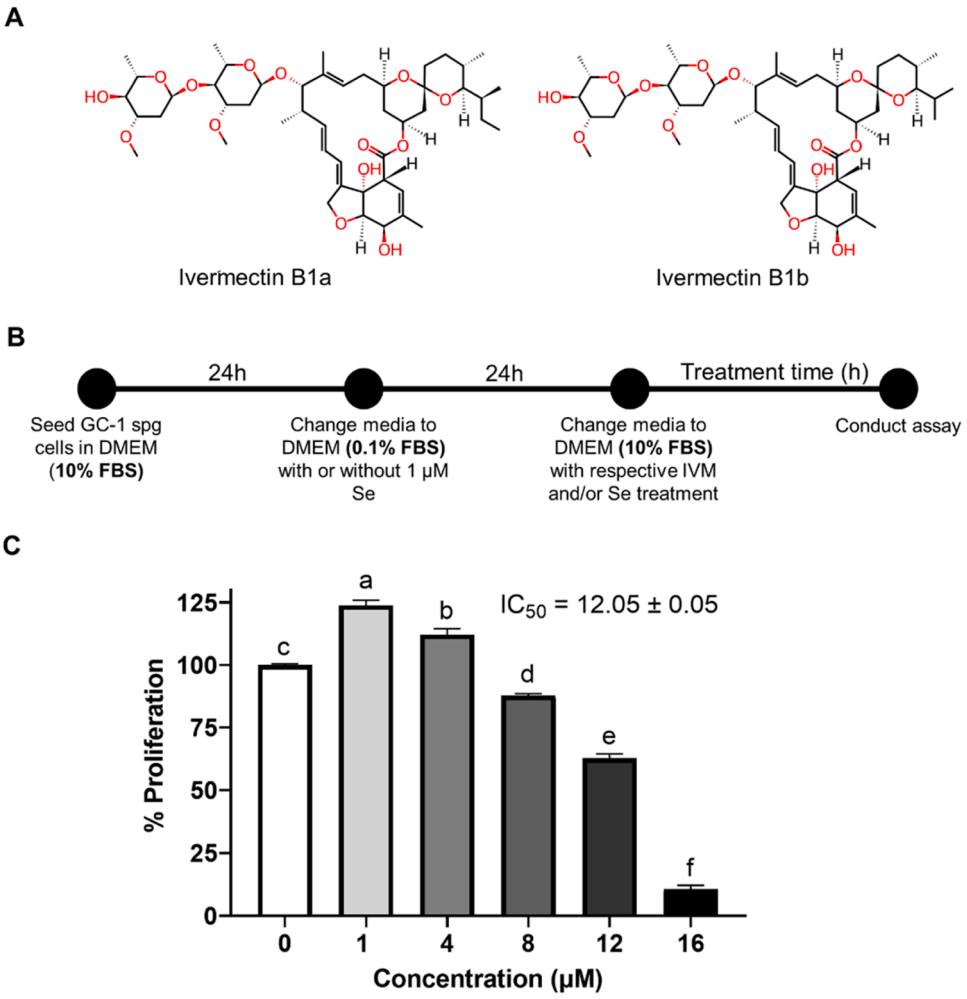


Fig. 1. Inhibition of proliferation of GC-1 spg cells treated with IVM for 24 h. (A) Molecular structure of IVM isomers. **(B)** Overview of the *in vitro* culture and treatment scheme used in this study. **(C)** Proliferation of GC-1 spg cells treated with various concentrations of IVM (n = 5). Data are presented as means ± SEM. Significant differences are indicated by different letters (a, b, c, d, e, and f) when $p < 0.05$.

Zhang et al., 2022). Thus, redox mechanisms are likely behind IVM-induced injuries in male germ cells.

Selenium (Se) is an essential trace element naturally found in food and synthetically added to supplements (Ye et al., 2021). Cells utilize bioavailable Se to synthesize and upregulate selenoprotein activity (Abo El-Magd et al., 2022). Seven out of 25 ER-localized selenoprotein families participate in regulating redox balance, Ca^{2+} flux, and protein folding, which are dysregulated processes during ER stress (Ding et al., 2022; Pitts and Hoffmann, 2018). ER stress upregulates the unfolded protein response (UPR) genes, which serve as its quantifiable indicators (Hetz, 2012; Oslowski and Urano, 2011).

This study presented the first molecular-level evidence of IVM's novel mechanism in inducing apoptosis via ER stress in GC-1 spg cells, an immortalized type B spermatogonia cell line from mouse. It also explored the mechanism in which inorganic Se in the form of sodium selenite (Na_2SeO_3) protects mouse spermatogonia from IVM-induced cytotoxicity by upregulating selenoproteins capable of restoring redox homeostasis. The findings of this mechanistic study offered insights into the extent of damage IVM exerts and possible interventions to alleviate IVM toxicity in male germ cells.

2. Materials and methods

2.1. GC-1 spg cell culture maintenance and experiment conditions

GC-1 spg cells (CRL-2053, American Type Culture Collection, Manassas, VA, USA) were cultured in Dulbecco's modified Eagle's medium (DMEM, L0103–500; Biowest, Nuaillé, France) supplemented with 10 % fetal bovine serum (FBS, S1480; Biowest) and 1 % penicillin and streptomycin (15140122, Gibco, Waltham, MA, USA). Cells were maintained in 100 mm culture dishes inside at 37°C in a humidified incubator with 5 % CO_2.

For experiments, cells were seeded in 100- or 60-mm culture dishes, or 6-well culture plates at a density of 20, 000 cells/mL in complete growth medium (phenol red-free DMEM (LM001–10; Welgene, Gyeongsan-si, Korea) supplemented with 10 % FBS, 1 % penicillin and streptomycin, and 1 % sodium pyruvate (Gibco)). After 24 h, the medium was removed, and cells were washed twice with 1× Dulbecco's Phosphate-Buffered Saline (DBPS, 14080055; Life Technologies, Grand Island, NY, USA). Cells were then incubated in quiescence medium (DMEM supplemented with 0.1 % FBS, 1 % penicillin and streptomycin, and 1 % sodium pyruvate) to synchronize them in low-serum conditions, thereby limiting hormones and growth factors prior to IVM treatment.

For Se treatment groups, the quiescence medium was supplemented with 1 μM Na_2SeO_3 (214485; Sigma-Aldrich, St. Louis, MO, USA). After 24 h, the quiescence medium was replaced with appropriate complete growth media based on the experimental group: 1, 4, 8, 12, or 16 μM IVM (18898; Sigma-Aldrich) for IVM groups, 1 μM Na_2SeO_3 for Se groups, or 1 μM Na_2SeO_3 combined with 16 μM IVM for Se and IVM co-treatment groups. The IVM used consisted of $\geq$ 90 % B1a and $\leq$ 5 % B1b. Cells were exposed to the respective conditions for the specified durations (Fig. 1B).

2.2. Proliferation measurement via trypan blue exclusion assay (TBEA)

TBEA was performed to measure the capability of GC-1 spg cells to proliferate in the presence of varying concentrations of IVM and/or in the presence or absence of Se. After 24 h of exposure to the respective conditions, the cells were collected using 0.25 % trypsin-ethylenediaminetetraacetic acid (EDTA) (25200072; Invitrogen, Carlsbad, CA, USA). The reaction was quenched in medium containing 10 % FBS. Cell suspensions were centrifuged at 600 × g for 6 min at 4°C, and the resulting pellets were resuspended in DPBS with 1 % FBS. Cells were then mixed in a 1:1 ratio with trypan blue solution (15250061, Gibco) and loaded onto a Neubauer hemocytometer. Viable cells (those unstained by trypan blue) were counted under the light microscope (Nikon Eclipse TS100, Japan). The percentage (%) proliferation and relative % proliferation were calculated as follows:

$$\%\text{Proliferation} = \frac{\text{Number of Harvested cells}}{\text{Number of Seeded cells}} \times 100$$

$$\text{Relative }\%\text{Proliferation} = \frac{\text{Proliferation}_{\text{X μM IVM}}}{\text{Proliferation}_{\text{0 μM IVM}}} \times 100$$

The half-maximal inhibitory concentration (IC_{50}) was determined from the calculated relative % proliferation data using the three-parameter formula for the sigmoid dose-dependent curves:

$$Y = \text{Bottom} + \frac{\text{Top} - \text{Bottom}}{1 + \left(\frac{IC_{50}}{X}\right)}$$

2.3. Detection of ROS generation using dichlorodihydrofluorescein diacetate (DCFDA)

Intracellular ROS were visualized using the fluorogenic probe DCFDA (D6883; Sigma-Aldrich) after 3 h of IVM treatment. Cells were washed twice with 1× DPBS and incubated in phenol-free DMEM containing 1 % FBS and 10 μM DCFDA for 45 min at 37°C. Cells were washed twice with cold DPBS containing 1 % FBS.

2.4. Visualizing cytosolic Ca^{2+}

Cytosolic Ca^{2+} levels were visualized using Fluo-4, AM (F14201; Sigma-Aldrich) after 3 h of IVM exposure. Cells were washed twice with phenol-, Ca^{2+}-, and Mg^{2+}-free DMEM. Fluo-4, AM (1 μM) in the same medium was added to the cells, followed by incubation for 1 h at 37°C. The cells were washed thrice and incubated with phenol-free DMEM for 30 min. Cold phenol-free DMEM was used to wash the cells before imaging.

2.5. Detection of ER stress

ER stress was detected 3 h after stimulation with IVM using a modified method based on Thioflavin T (ThT) staining and fluorescence microscopy by Beriault and Werstuck (2013). To stain the cells, 5 μM ThT (T3516; Sigma-Aldrich) was added to the final complete growth medium with respective treatments, and cells were incubated for 3 h at 37°C. Cells were then washed once with cold DPBS containing 1 % FBS.

2.6. Semi-quantitation of fluorescence microscopy images

Fluorescence microscopy images of cells stained with DCFDA, Fluo 4-AM, or ThT were captured using a TE2000-U fluorescence microscope with NIS element imaging software (Nikon, Tokyo, Japan). Fluorescence signals from cells stained with DCFDA, Fluo 4-AM, or ThT were semi-quantified using ImageJ v1.54 h software (National Institutes of Health, Bethesda, MD, USA), which calculated the % area of fluorescence for each image. The red, green, and blue (RGB) images were converted to 16-bit grayscale and then 8-bit binary images by setting a threshold to isolate only fluorescent areas. The total number of cells per image was counted manually, with five random fields analyzed per replicate. The following formula, adapted from Beriault and Werstuck (2013), was used to normalize fluorescence data to the number of cells in each image:

$$\%\text{Area of fluorescence per 100 cells} = \frac{\%\text{Area}}{\text{Total number of cells in the field}} \times 100$$

2.7. Live cell timelapse imaging

To observe changes in cell morphology over time following IVM exposure, a Lumascope 850 microscope and LumaViewPro software (Etaluma, San Diego, CA, USA) were utilized. After treatment, plates were placed on a microscope stage within an incubator set at 37°C in 5 % CO_2. Five random fields were imaged for each replicate, capturing one brightfield photograph every 5 min for a total of 3 h. Time-lapsed videos were generated using ImageJ v1.54 h software.

Supplementary material related to this article can be found online at doi:10.1016/j.ecoenv.2024.117307.

2.8. Quantifying apoptotic cells via Annexin V/Propidium iodide (AV/PI) apoptosis assay

To quantify apoptotic cells resulting from IVM and/or Se exposure, dual staining with allophycocyanin (APC)-conjugated AV (550475; BD Biosciences, San Jose, CA, USA) and propidium iodide (PI) was performed after 3 h of treatment. Cells were harvested using 0.25 % trypsin-EDTA and then quenched in medium supplemented with 10 % FBS. Following centrifugation at 600×g for 6 min at 4°C, the cells (0.1×10^6) were resuspended in 100 µL of 1× binding buffer (BD Biosciences) containing 5 µL APC-conjugated AV and 2 ng/mL PI. Cells were agitated in the dark on an orbital shaker at 21°C for 15 min. Cell suspensions were diluted with 400 µL binding buffer before being loaded into FACSAria™ II cell sorter (BD Biosciences). Flow cytometry results were analyzed using FlowJo v10.8.1 (BD Life Sciences).

2.9. Quantitative reverse transcription-polymerase chain reaction (qRT-PCR)

After 3 h of treatment, RNA was extracted by collecting and lysing cells in low-pH TRIzol™ reagent (Invitrogen, Waltham, MA, USA). Total RNAs were purified further using HiGene™ Total RNA Prep Kit (RP101; BioFACT, Daejeon-si, Korea). Isolated total RNAs were assessed for purity and quantity using NanoDrop One spectrophotometer (Thermo Fisher Scientific, Waltham, MA, USA). Complementary DNAs were synthesized by loading 5000 ng of total RNA in a BioFACT™ RT-KIT (BR122; BioFACT). Specific primers (Table S1) were designed for detection and quantification of the housekeeping genes *Glyceraldehyde-3-phosphate dehydrogenase* (*Gapdh*) and *Peptidylprolyl isomerase A* (*Ppia*), extrinsic apoptosis-related genes *Tumor necrosis factor alpha* (*Tnfα*) and *Fas receptor* (*Fas*), intrinsic apoptosis-related genes *B cell leukemia/lymphoma 2* (*Bcl2*) and *BCL2-associated X protein* (*Bax*), ER stress-mediated apoptosis-related genes *C/EBP homologous protein* (*Chop*) and *Activating transcription factor 4* (*Atf4*), selenoprotein-encoding genes including *Glutathione peroxidase 1* (*Gpx1*), *Glutathione peroxidase 4* (*Gpx4*), *Selenoprotein H* (*Selenoh*), *Selenoprotein K*, *Selenoprotein M* (*Selenom*), *Selenoprotein O* (*Selenoo*), *Selenoprotein S* (*Selenos*), *Selenoprotein T* (*Selenot*), and *Selenoprotein V* (*Selenov*), mitochondria-associated endoplasmic reticulum membrane (MAM) genes *Inositol 1,4,5-trisphosphate receptor 1* (*Ip3r1*), *Glucose-regulated protein 75* (*Grp75*), and *Voltage-dependent anion channel 1* (*Vdac1*), and the UPR genes *Glucose-regulated protein 78* (Grp78) and *Ubiquitin-like domain member 1* (*Herpud1*).

qRT-PCR was performed using 2× SYBR Green PCR Master Mix with low ROX reference dye (DQ384; BioFACT) in an ABI PRISM 7500 Real-Time PCR System (Applied Biosystems, Carlsbad, CA, USA) in 96-well plates (N8010560; Applied Biosystems) and CFX Opus 96 Real-Time PCR System (Bio-Rad Laboratories, Hercules, CA, US) in 96-well plates (HSP9601; Bio-Rad Laboratories). The cycling conditions included an initial holding stage at 95°C for 15 min, followed by 40 cycles of 95°C for 20 s and 60°C for 40 s. Melting curves were determined at the end using a protocol of 95°C for 15 s, 60℃ for 1 min, 95℃ for 30 s, and 60℃ for 15 s. Gene expression was quantified using the $2^{-\Delta\Delta Ct}$ method.

2.10. Western blotting

GC-1 spg cells were scraped, collected, and centrifuged for 6 min at 600×g at 4°C after 3 h of treatment. The cell pellets were resuspended in cold DBPS and centrifuged for 1 min at 19000×g. The pellets were then resuspended in Total Extraction buffer (Shin et al., 2014) supplemented with 1 mM dithiothreitol, 0.5 mM phenylmethylsulfonyl fluoride, and Halt™ protease inhibitor cocktail (1862206; Thermo Fisher Scientific). The cell suspensions were pipetted vigorously before being submerged in liquid nitrogen for flash freezing. After thawing in room temperature water, the suspensions were briefly vortexed and flash frozen. The freeze–thaw cycle was repeated 10 times.

After the last thawing step, the suspensions were centrifuged at 19000×g for 30 min at 4°C. The supernatants were collected and protein concentrations were quantified using the Bradford assay (5000006; Bio-Rad, Hercules, CA, USA). Equivalent quantities of protein, along with a protein ladder marker (SM306; BioFACT), were loaded and run on a hand-cast, triple percentage gradient sodium dodecyl sulfate-polyacrylamide gel (6, 12, 15 %; 3:4:3). After gel electrophoresis, the proteins were transferred onto Immobilon®-P polyvinylidene difluoride membranes (IPVH00010; Millipore, Billerica, MA, USA), which were pre-activated for 1 min with 100 % methanol (322415, purity >99.8 %; Sigma-Aldrich).

The membranes containing the transferred blots were submerged in 5 % skim milk in DPBS containing 0.2 % Tween 20 (PBS-T) and shaken for 30 min at room temperature. After a brief wash with PBS-T, the membranes were incubated with primary antibodies at 4°C for at least 8 h. The membranes were then washed three times with PBS-T and incubated with their respective secondary antibodies (either anti-mouse IgG or anti-rabbit IgG) for 2 h at room temperature. The antibodies used in this study are listed in Table S2. To visualize the blots, the membranes were washed three times and then momentarily submerged in West-Glow™ Femto solution (BWF0100; Biomax, Guri-si, Korea) for a maximum of 5 s before scanning with an e-Blot Touch Imager (e-Blot Life Science, Shanghai, China).

2.11. Statistical analysis

Statistical analyses were performed using GraphPad Prism v9.5.1 (GraphPad, La Jolla, CA, USA). Every experiment was conducted in at least 3 biological replicates. Data are presented as the mean ± standard error of the mean (SEM). Multiple comparison analysis was performed using one-way analysis of variance, followed by Tukey's Honest Significant Difference post-hoc test at a 5 % significance level. Significant differences are presented through a compact letter display (CLD) in which groups assigned with different letters indicate statistical significance ($p < 0.05$).

3. Results

3.1. IVM dose-dependently inhibits proliferation in mouse spermatogonia within 24 h

In vitro proliferation of mouse type B spermatogonia was assessed after 24 h of treatment to allow one cell cycle before measurement. At low IVM concentrations (1–4 µM), a significant increase of proliferation was observed. At higher doses of IVM, cell proliferation decreased in a dose-dependent manner, eliciting a dose-response sigmoid curve. The highest cell proliferation of approximately 1.2-fold of the untreated group was observed with 1 µM IVM. In contrast, the lowest proliferation was seen in cells treated with the highest IVM concentration (16 µM). The IC_{50} was determined to be 12.05 ± 0.05 (Fig. 1C). We selected the concentrations below and above IC_{50} (8 and 16 µM, respectively) for further assays to elucidate the molecular mechanisms of IVM cytotoxicity in GC-1 spg cells.

3.2. IVM induces dose-dependent redox dysregulation and ER stress in mouse spermatogonia within 3 h

Redox homeostasis imbalances and ER stress in GC-1 spg cells subjected to IVM for 3 h were determined. Fluorescence microscopy of DCFDA-, Fluo-4 AM-, and ThT-stained GC-1 spg cells revealed dose-dependent increases in intracellular ROS, cytosolic Ca^{2+}, and misfolded proteins. Untreated cells showed minimal fluorescence, whereas cells treated with 8 μM IVM showed intermediate intensity of fluorescence. Cells exposed to 16 μM IVM exhibited the most intensity (Fig. 2A–F). UPR gene upregulation, a downstream phenomenon of ER stress, was quantified via gene expression changes in *Grp78* (the master regulator of UPR), *Chop* and *Atf4* (UPR genes that dictate the fate of ER-stressed cells towards apoptosis), and *Herpud1* (a UPR gene that is solely upregulated via ER stress). All genes exhibited a similar pattern of upregulation in response to increasing IVM doses, with significant increases observed only in cells treated with 16 μM IVM groups. For *Grp78,* mRNA expression increased dose-dependently, with significant changes noted in both 8 μM and 16 μM IVM groups (Fig. 2G). This dose-dependent trend was also reflected in the protein levels of Grp78 and Chop (Fig. 2H). Regarding the Ip3r1-Grp75-Vdac1 axis, only Grp75 showed a significant increase in both mRNA and protein levels with increasing IVM concentrations (Fig. 2G and H).

3.3. IVM rapidly and dose-dependently induces apoptosis in mouse spermatogonia within 3 h

Live cell imaging of IVM-treated GC-1 spg cells was conducted to investigate the changes in morphology as a function of dose and time. Changes in morphology were negligible in cells treated with 8 μM. In contrast, multiple cells exhibited hallmarks of early apoptotic morphology (i.e., shrinking and blebbing) as early as 1 h after exposure to 16 μM IVM. Beyond that time, the cells rapidly transitioned from early apoptotic to late apoptotic or secondary necrosis morphology between 2 and 3 h timepoint (Fig. 3A and Supplementary Content 1 and 2).

The protein and mRNA levels of apoptosis regulators were investigated to clarify the mechanisms of cell death. Activation of Caspase-9 (activated by ER stress and Cytochrome c release), Caspase-8 (activated via death ligand signaling), and Caspase-3 (the main executor of apoptosis), were observed only in cells treated with 16 μM IVM. B-cell lymphoma 2 (Bcl-2), a regulator of Ca^{2+} homeostasis in the mitochondria and the ER and inhibitor of Cytochrome c release, decreased in cells exposed to 16 μM IVM. Bax, which promotes Cytochrome c release, increased in the same concentration. Both Bcl-2 and Bax decreased in cells treated with 8 μM IVM. However, Cytochrome c was virtually depleted and Bcl-2/Bax ratio significantly dropped only in 16 μM IVM-treated cells (Fig. 3B and C). These effects occurred between the 2–3 h timepoint, temporally coinciding with the accumulation of apoptotic cells in the timelapse video (Figure S2 and Supplementary Content 2).

The mRNA encoding for the death ligand Tnf-α and death ligand receptor Fas increased only in cells treated with 16 μM IVM (Fig. 3C). AV- and PI-positive cells, which represent the population of late apoptotic cells, were observed in cells treated with 16 μM IVM, compared to untreated cells and cells treated with 8 μM IVM after 3 h (Fig. 3D-E).

3.4. Se stimulates proliferation in mouse spermatogonia exposed to IVM for 24 h

A previous report suggested that commercial veterinary Se and vitamin E supplements in murine models treated with IVM can rescue testicular function (Ahmed et al., 2020). Therefore, the second phase of this study focused on investigating the rescue mechanism of the cotreatment of 1 μM Se in GC-1 spg cells treated with 16 μM *in vitro*. Adding Se significantly enhanced the proliferation of cells in cotreatment group compared to those treated with IVM alone. In addition, there was no significant difference in the proliferation of untreated cells and cells treated with Se alone (Fig. 4B, S4).

3.5. Se alleviates redox dysregulation and ER stress in mouse spermatogonia exposed to IVM for 3 h

Since Se improved the general cytotoxicity parameters of IVM-treated mouse spermatogonia, we investigated the mechanism of action of Se against IVM-induced redox imbalance and ER stress. Cotreatment with Se and IVM significantly decreased the fluorescence intensity of DCFDA-stained GC-1 spg cells compared to the intensity of cells treated with solely IVM, while cells treated with Se alone exhibited negligible fluorescence like untreated cells (Fig. 5A and D). Regarding the Ca^{2+} levels in the cytosol, cotreatment with Se and IVM significantly decreased the fluorescence intensity versus those treated with only IVM. Untreated and Se-treated groups exhibited low fluorescence intensity (Fig. 5B and E). ThT fluorescence results showed that while IVM singly induced the most significant increase in fluorescence, cells cotreated with Se and IVM had a fluorescence intensity like the untreated cells. Cells solely treated with Se showed a slight increase in fluorescence compared to untreated cells (Fig. 5C and F). Se and IVM-treated group had significantly decreased expressions of *Grp75, Grp78*, *Atf4*, *Chop*, and *Herpud1* genes compared to those treated with IVM only. The same can be said in the protein levels of Grp75, Grp78, and Chop (Fig. 5H). The mRNA levels of UPR genes in cotreated cells were not statistically significant compared to those in untreated cells and cells treated with Se alone (Fig. 5G).

To explore the molecular mechanisms by which Se alleviates redox dysregulation and ER stress, we screened a group of selenoprotein-encoding genes for expression changes (Fig. 5I and S1). In cells treated with both IVM and Se, we observed a significant upregulation of the five genes encoding *Gpx1* (reduces intracellular hydrogen peroxide), *Gpx4* (testis-enriched, reduces lipid peroxides), *Selenoh* (responds to redox imbalances by upregulating the expression of genes involved in glutathione synthesis and phase II detoxification), *Selenom*, (ER-resident, reduces superoxides, regulates disulfide bond formation, and maintains Ca^{2+} homeostasis), and *Selenov (*testis-specific, possibly restores redox homeostasis based on protein structure) (Pitts and Hoffmann, 2018; Z. Zhang et al., 2019). *Gpx4* and *Selenov* were not upregulated by Se alone, unlike *Gpx1*, *Selenoh*, and *Selenom*. While there was a >10-fold decrease in *Selenov* expression in GC-1 spg cells solely treated with Se compared to untreated cells, it was not statistically significant (Fig. 5H).

3.6. Se mitigates IVM-induced apoptosis in mouse spermatogonia within 3 h

We investigated the levels of apoptosis regulators in GC-1 spg cells after adding Se to determine whether the alleviation of redox imbalance and ER stress can mitigate apoptosis. Cleaved Caspase-9, −8, and −3 were relatively lower in cells treated with IVM and Se than in cells treated with IVM alone. Bcl-2 levels remained stable in the cotreated cells, whereas it decreased in cells treated with IVM alone; likewise, Bax levels did not increase. Furthermore, cotreated cells exhibited substantially higher Cytochrome c levels compared to IVM-only treated cells (Fig. 6A). Cells cotreated with Se and IVM showed significantly higher expression of *Bcl-2* and lower expressions of the *Bax, Tnfα* and *Fas* genes compared to cells solely treated with IVM (Fig. 6B).

4. Discussion

Multiple animal studies describe IVM's deleterious effects on male fertility, even at therapeutic doses (Ahmed et al., 2020; Cordeiro et al., 2018; EL-Maddawy and Abd El Naby, 2018; El-Nahas and El-Ashmawy, 2008; El-Shobokshy et al., 2023). Amid the abundance of *in vivo* studies on IVM toxicity, *in vitro* studies remain relevant by demonstrating

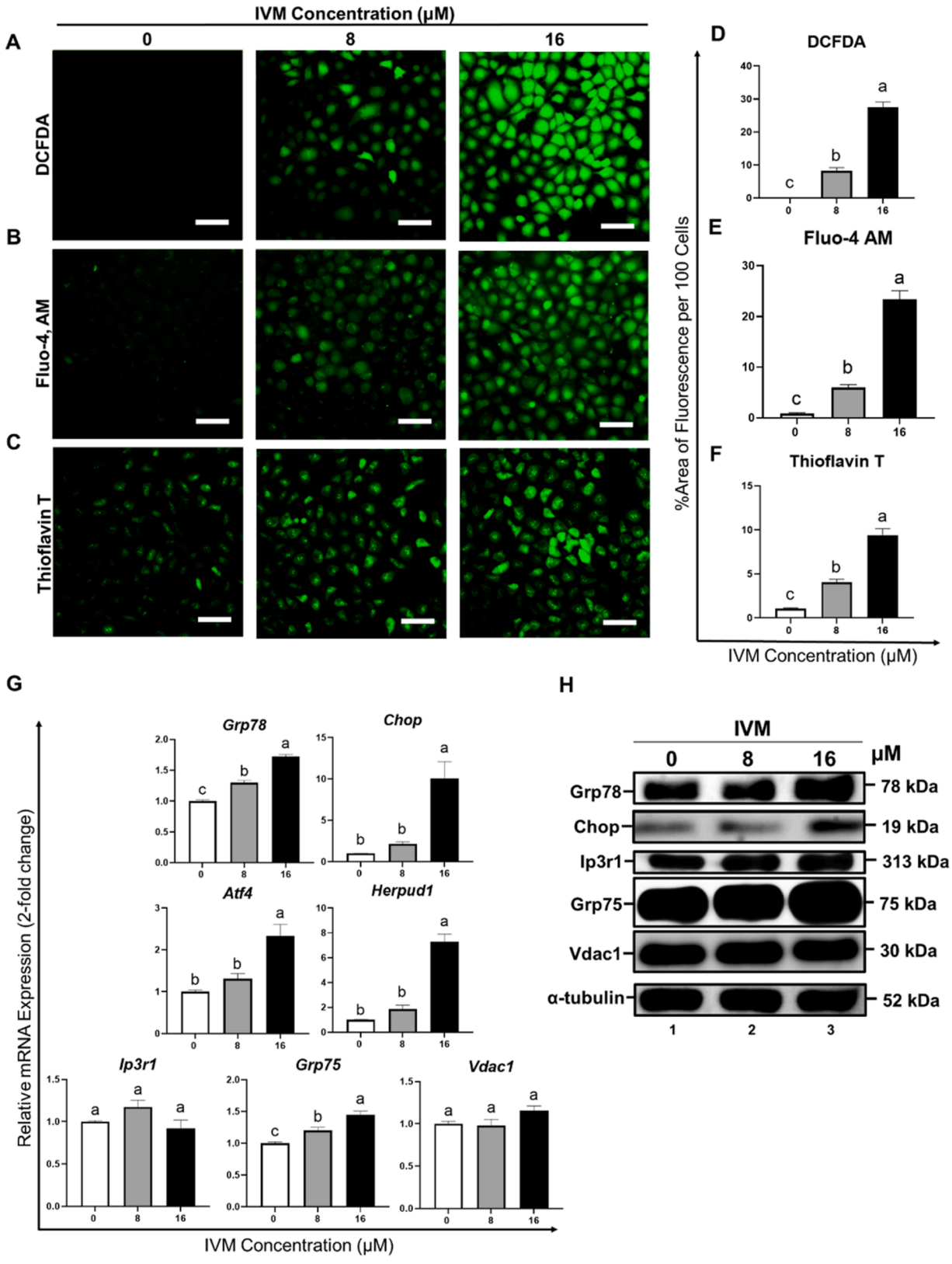


Fig. 2. Dose-dependent redox dysregulation and ER stress in GC-1 spg cells treated with IVM for 3 h. Fluorescence microscopy images of GC-1 spg cells stained with **(A)** DCFDA, **(B)** Fluo-4 AM, **(C)** and ThT. Semi-quantification of fluorescence intensity based on five random fields-of-view for GC-1 spg cells stained with **(D)** DCFDA, **(E)** Fluo-4 AM, and **(F)** ThT (n = 3). **(G)** Fold changes in ER stress-related genes of GC-1 spg cells treated with 0, 8, and 16 μM IVM (n = 3). **(H)** Changes in ER stress-related protein levels of GC-1 spg cells treated with 0, 8, and 16 μM IVM (n = 3). Scale bar: 100 μm. Data are presented as means ± SEM. Significant differences are indicated by different letters (a, b, and c) when $p < 0.05$.

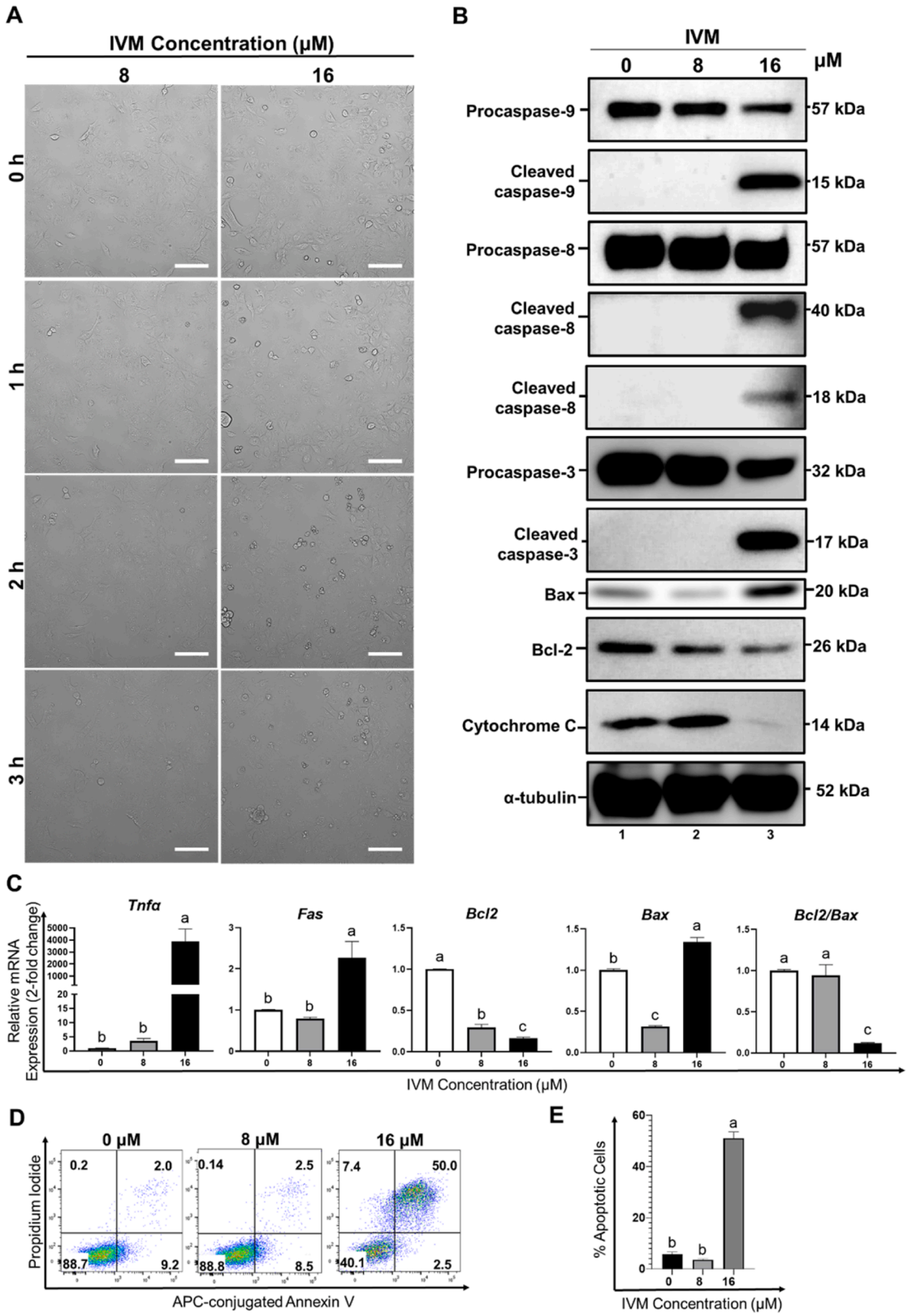


Fig. 3. Time- and dose-dependent caspase activation and apoptosis in GC-1 spg cells treated with IVM for 3 h. (A) Timelapse live cell imaging of IVM-treated GC-1 spg cells. **(B)** Western blots of apoptosis-related markers of GC-1 spg cells treated with 0, 8 and 16 μM IVM (n = 3). **(C)** Fold changes in apoptosis-related gene expression of GC-1 spg cells (n = 3). **(D)** Representative dot plots and **(E)** quantified apoptotic cells of GC-1 spg cells double-stained with allophycocyanin-conjugated Annexin V and propidium iodide (n = 3). Scale bar: 100 μm. The data are presented as means ± SEM. Significant differences are indicated by different letters (a, b, and c) when $p < 0.05$.

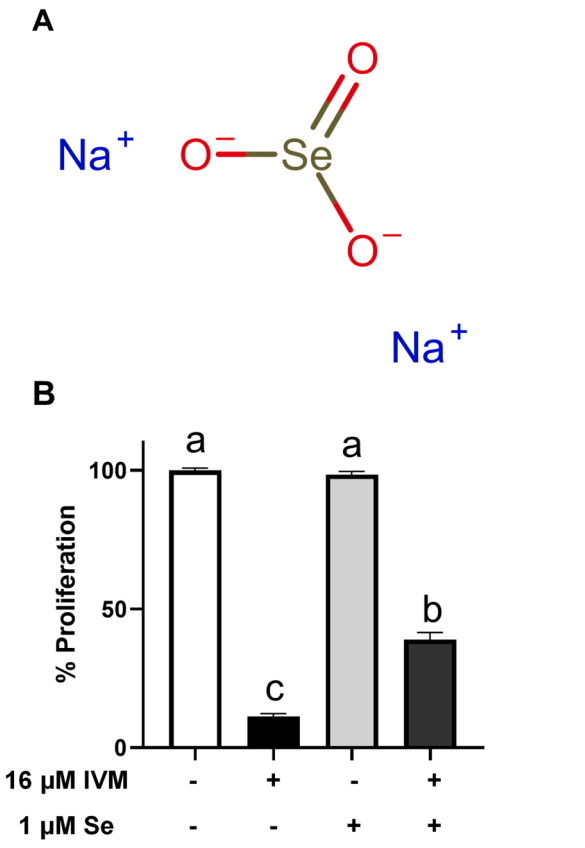


Fig. 4. Rescue of proliferation in GC-1 spg cells pretreated with Se for 24 h, followed by cotreatment with IVM and Se for 24 h. (A) Molecular structure of Na_2SeO_3. **(B)** Proliferation of GC-1 spg cells treated with IVM and/or Se (n = 5). The data are presented as means ± SEM. Significant differences are indicated by different letters (a, b, and c) when $p < 0.05$.

molecular mechanisms in rigorous detail using live type B spermatogonia. This study highlights the dose-dependent toxicity of IVM in type B spermatogonia as exhibited by the loss of proliferation as the concentration increases. In concentrations beyond IC_{50}, IVM rapidly induces apoptosis within 3 h of drug exposure. This rapid programmed cell death is highly associated with oxidative stress, subcellular Ca^{2+} dysregulation, and protein misfolding. Mitochondrial dysfunction mediates apoptosis via these stressors due to mitochondrial Ca^{2+} overload through MAM's Grp75. Se inhibits these upstream stressors by upregulating selenoprotein-encoding genes which maintain the homeostasis of the subcellular redox environment, resulting to an improvement in proliferation of cells treated with high concentrations of IVM. This confirms the interplay of these events in the toxicological mechanism of IVM in type B spermatogonia.

In vivo studies report imbalances in levels of reduced glutathione and malondialdehyde, as well as the loss of activity of antioxidative enzymes, such as catalase and superoxide dismutase (Ahmed et al., 2020; Cordeiro et al., 2018; EL-Maddawy and Abd El Naby, 2018; El-Nahas and El-Ashmawy, 2008; El-Shobokshy et al., 2023). These results are consistent with the dose-dependent oxidative stress we observed, except ER stress adds nuance to the mechanism. Protein folding lies on the delicate redox balance on a subcellular level. In homeostatic cells, the cytosol is a relatively reducing environment compared to organelles such as the ER, which holds a more oxidizing environment to fold proteins. Thus, slight redox shifts may challenge the cell's homeostasis (Cao and Kaufman, 2014; Lee et al., 2019). Therefore, extremely oxidating conditions from high concentrations of IVM affect the ER's functions in type B spermatogonia. The cell's sensitivity to redox changes may also explain the slight increase in ThT fluorescence in cells treated with Se alone. Se can amplify reducing reactions by acting as cofactor for glutathione peroxidases (Nancharaiah and Lens, 2015; Zoidis et al., 2018) and upregulating selenoprotein-encoding gene expression in type B spermatogonia. However, it was not accompanied by a significant induction of UPR nor a decrease of cell proliferation. Hence, while Se can promote a more reducing environment enough to restore homeostasis in type B spermatogonia under oxidative stress, it does not induce ER stress alone and at low doses.

A recent study that screened small molecules that preserve mitochondrial ATP in hypoxic human-induced pluripotent stem cell-derived cardiomyocytes noted that low IVM concentrations upregulates pro-survival UPR via *Chop* and *Atf4* to prevent loss of mitochondrial ATP (Nagai et al., 2017). IVM's ability to modulate mitochondrial activity at relatively low doses may explain why both Bcl-2 and Bax were transcriptionally and post-translationally downregulated in 8 μM-treated type B spermatogonia. These cells survived since a decrease of Bcl-2/Bax ratio was not observed. The study's findings also raise the question of whether the IVM ability to induce UPR is linked to cell death. Herein, the inhibition of UPR genes and apoptosis regulators led to improved general cytotoxicity parameters by Se in IVM-treated cells, strongly suggesting that under these conditions, UPR is not pro-survival but rather drives apoptosis. It could also be argued that the misfolded proteins and UPR that were observed may be caused by oxidative stress without stressing the ER, and that the disruption of Ca^{2+} homeostasis may be solely a mitochondrial event. However, the significant upregulation of *Herpud1* induced by ER stress, and not oxidative stress, strongly supports the hypothesis that ER stress occurs in mouse spermatogonia affected by IVM (Ho and Chan, 2015).

In IVM's toxicological mechanism in type B spermatogonia, the link between ER stress and apoptosis comprises not only protein misfolding, but also intracellular Ca^{2+} signaling. Grp75 tethers the Ip3r1 found in the MAM with the ion channel Vdac1 located in the outer mitochondrial membrane. Changes in Grp75 level and activity are known to control the cell fate in specific contexts (Li et al., 2022; Ma et al., 2023; Tiwary et al., 2021). The increase of transcriptional and posttranslational expression of Grp75 in high doses of IVM suggests that aside from the cytosol, the mitochondria also experience Ca^{2+} overload, which causes mitochondrial dysfunction, generates more ROS, and triggers apoptosis. Se inhibits this increase in Grp75 expression, which leads to the inhibition of apoptosis and improvement in cell proliferation. Thus, IVM increases MAM activity to exacerbate IVM toxicity in type B spermatogonia.

The stressors amplify each other over a short time using this mechanism, leading to an interesting induction of apoptosis in type B spermatogonia. The protein levels of mitochondria-associated apoptosis follow intrinsic apoptosis, but the Cytochrome c is dose-dependently decreasing. For intrinsic apoptosis to occur, Cytochrome c must be released via the downregulation of mitochondrial Bcl-2 and upregulation of Bax. Cytosolic Cytochrome c then complexes with the apoptosome to activate caspase-9 and promotes the cascading cleavage of caspases. Unlike the reports of previous studies reporting apoptosis as a consequence of toxicity in GC-1 spg, the total cytochrome C levels were depleted instead of accumulated (Kim et al., 2024; R. Lee et al., 2022). These studies utilize toxicants that induce apoptosis at 24 h, while IVM rapidly triggers apoptosis within 2–3 h. Sudden and intense stress coupled by the rapid transition of cells towards late apoptosis most likely caused an extracellular release of Cytochrome c (Gouveia et al., 2017; Javid et al., 2015; Renz et al., 2001). On the other hand, the released Cytochrome c may also be subject to degradation pathways. Given the pace of apoptosis in IVM-treated type B spermatogonia, the proteolytic degradation of the released Cytochrome c by high caspase activity may be accelerated as well. Either of the two scenarios may further complicate the detection of Cytochrome c in this study.

Despite the observed loss of total Cytochrome c, the cells continue to undergo apoptosis. The simultaneous decrease in levels of Cytochrome c and Bcl-2/Bax ratio and increase of fully cleaved Caspase-9 are time-coordinated in high doses of IVM. This corresponds to the observed

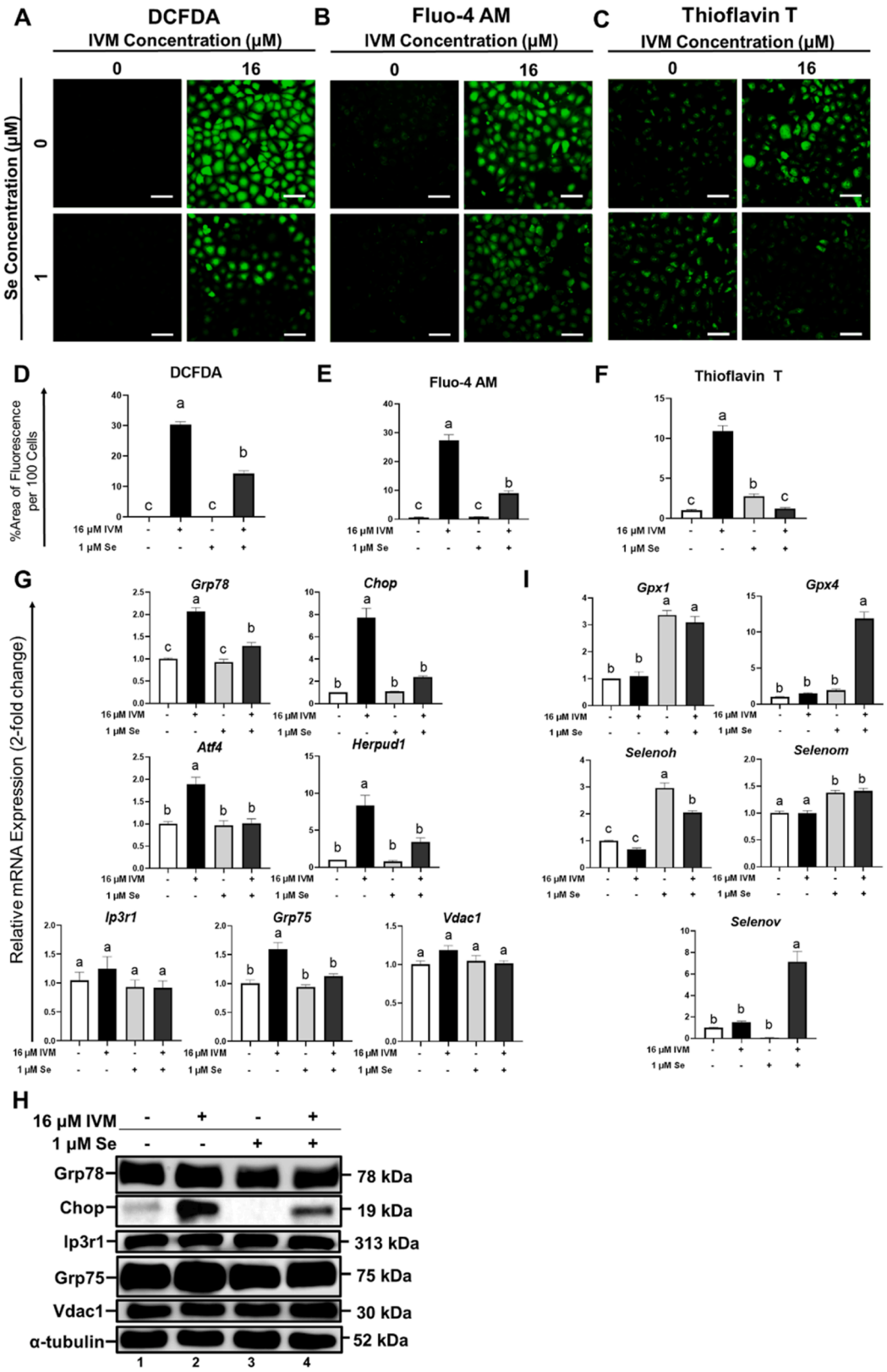


Fig. 5. Alleviation of redox dysregulation and ER stress in GC-1 spg cells pretreated with Se for 24 h, followed by cotreatment with IVM and Se for 3 h. Fluorescence microscopy images of GC-1 spg cells stained with **(A)** DCFDA, **(B)** Fluo-4 AM, and **(C)** ThT. Semi-quantified fluorescence intensity based on five random fields-of-view taken from GC-1 spg cells stained with **(D)** DCFDA, **(E)** Fluo-4 AM, and **(F)** ThT (n = 3). Changes in ER stress-related **(G)** gene expression and **(H)** protein levels (n = 3). **(I)** Fold changes in selenoprotein-encoding gene expression of GC-1 spg cells (n = 3). Scale bar: 100 μm. The data are presented as means ± SEM. Significant differences are indicated by different letters (a, b, and c) when $p < 0.05$.

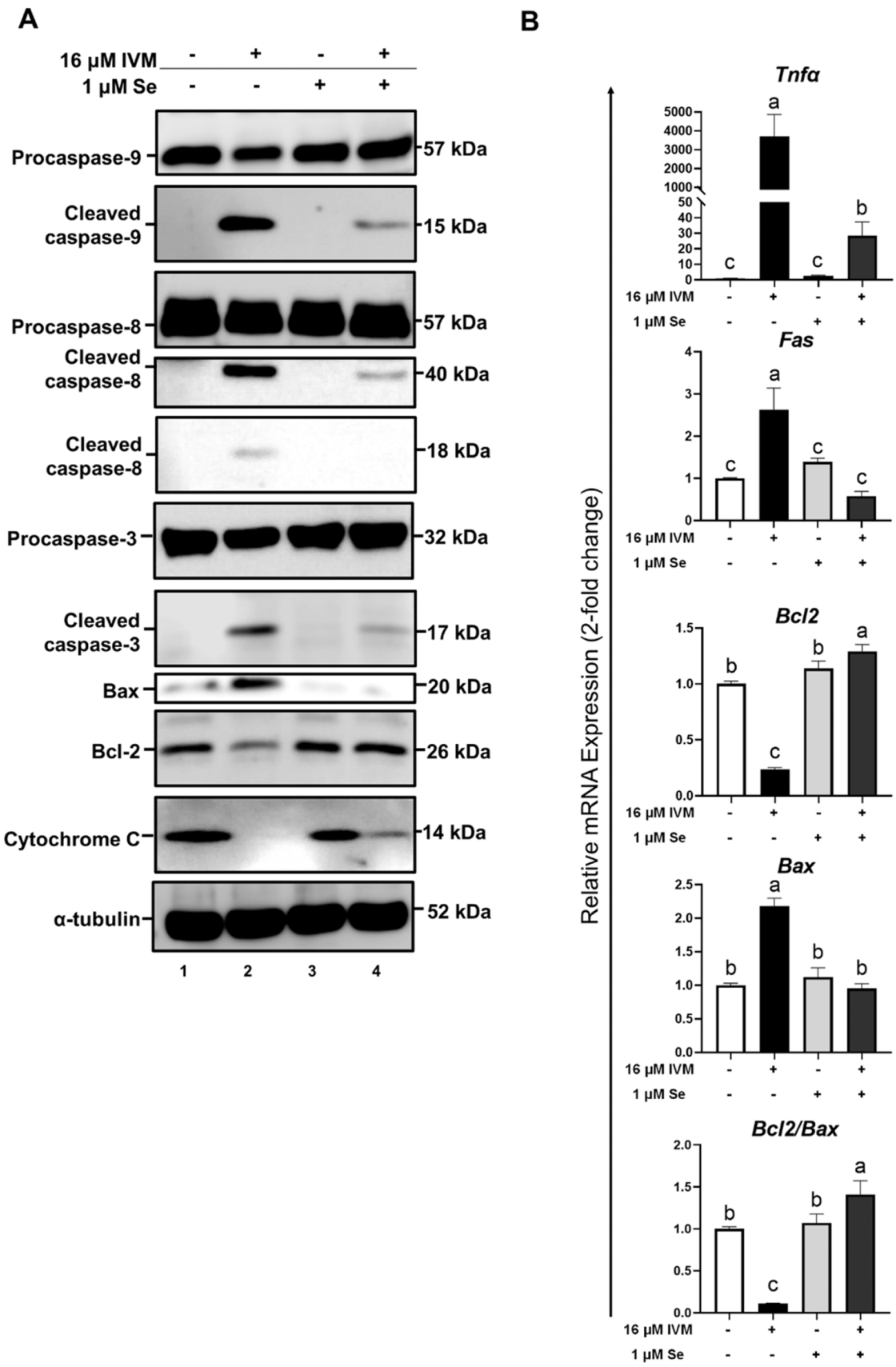


Fig. 6. Mitigation of caspase activation and apoptosis in GC-1 spg cells pretreated with Se for 24 h and cotreated with IVM and Se for 3 h (A) Western blots of apoptosis-related markers of GC-1 spg cells (n = 3). **(B)** Fold changes in apoptosis-related gene expression of GC-1 spg cells (n = 3). The data are presented as means ± SEM. Significant differences are indicated by different letters (a, b, and c) when $p < 0.05$.

accumulating number of cells undergoing morphological changes in the timelapse video. Cytochrome c, however, is restored by Se along with caspase cleavage inhibition and type B spermatogonia proliferation. These observations serve as evidence that the decrease of Cytochrome c remains associated with intrinsic apoptosis in this context. On the other hand, extrinsic apoptosis evident by the upregulation of *Tnfα* and *Fas* and caspase-8 activation is likely induced by intense oxidative stress, though *Tnfα* expression can also be upregulated by ER stress (Chipurupalli et al., 2021).

A previous study showed that supplementation with commercial Se and vitamin E mitigates IVM-induced testicular dysfunction *in vivo* (Ahmed et al., 2020). In the present study, Na_2SeO_3 was solely used as a rescue molecule to focus only on the factors attributed to Se when elucidating the molecular mechanisms of IVM-induced toxicity. Se reduced ROS and cytosolic Ca^{2+}, restored proper protein folding, and prevented UPR. However, Se cannot restore proliferation above and within the calculated IC_{50} (Figure S3) Therefore, it is logical to conclude that Se mitigates apoptosis led by high doses of IVM in mouse spermatogonia. These observations reflect the molecular consequences of the antioxidative action of Se and its ability to restore homeostasis.

IVM's trifecta of stressors can be mitigated by selenoproteins (Byun and Kang, 2011). Selenoproteins involved in protein folding homeostasis have a CxxU motif that reduces oxidized thioredoxin to restore proper folding and/or scavenge H_2O_2 (Alokda and Van Raamsdonk, 2023). Selenom can regulate the Ca^{2+} storage in male germ cells' ER in the presence of oxidative stress (Reeves et al., 2010; Varlamova et al., 2022). Glutathione peroxidase selenoproteins can utilize GSH to scavenge free radicals in male germ cells. However, Gpx1 and Gpx4 have different functional niches. Gpx1 has the preferential ability to reduce lipid peroxides in complex lipids. Gpx4, especially mitochondrial Gpx4, is highly enriched and indispensable in the testis (Brigelius-Flohé and Maiorino, 2013; L. Chen et al., 2021; Liu et al., 2023). Another special selenoprotein in the testis is Selenov owing to its tissue-specific expression. Although its function in the testes remains poorly understood, its CxxU motif participates in redox regulation, similar to other selenoproteins (L.-L. Chen et al., 2021; Liu et al., 2023). Its overexpression protects 293 T epithelial cells from oxidative and ER stress, whereas its knockout in hepatocytes predisposes them to stress-related injuries (Zhang et al., 2020). Its specific mechanism of function in the testes and its possible applications to male fertility, however, remains to be studied.

IVM-induced stressors or Se supplementation alone did not upregulate *Gpx4* or *Selenov*, but they were highly expressed in the presence of IVM and Se. These findings suggest that if Se were bioavailable, these genes respond to redox-related stresses in the testis. The function of *Gpx4* in alleviating oxidative stress from lipid peroxidation is well-documented. However, the same could not be said for *Selenov* prior to this study. The present results corroborate the recent finding that Selenov protects against oxidative and ER stress and their consequent injuries (L.-L. Chen et al., 2021). Additionally, the findings suggest increasing Se bioavailability as a therapeutic approach against redox imbalance-related concerns in the testis.

The determined IC_{50} of IVM toxicity in mouse spermatogonia is lower than the IC_{50} values reported in multiple *in vitro* studies that explored the antineoplastic potential of IVM (Chen et al., 2020; Dou et al., 2016; Jawad and Richardson, 2023; D. E. Lee et al., 2022; Tung et al., 2022; N. Xu et al., 2021; Zhang et al., 2022; Zhu et al., 2017). This implies that male reproductive toxicity may supersede intended effects in efforts to repurpose IVM for therapeutic use beyond helminthiasis. On the other hand, pharmacokinetic modeling suggested that 2 μM IVM in *in vitro* systems reportedly correspond to >35 times the maximum plasma concentration after oral intake of a single 200 μg/kg IVM dose (Schmith et al., 2020). Thus, the range of IVM concentrations that affect proliferation and cause cell death in mouse spermatogonia *in vitro* requires careful consideration before extrapolation, especially in environmentally relevant concentrations.

A significant increase in proliferation was observed in mouse spermatogonia stimulated for 24 h with low IVM concentrations. This observation is consistent with those of recent studies that defined the proliferative effects in cells treated with nanomolar, environmentally relevant concentrations of endocrine-disrupting chemicals, such as phthalates and bisphenol analogs (Cao et al., 2023; Lei et al., 2019). Hence, it would be beneficial for future studies to rule out the potential of IVM as an endocrine-disrupting chemical (European Food Safety Authority (EFSA) et al., 2022; Vandenberg et al., 2012).

5. Conclusion

IVM, though widely regarded as a 'wonder drug,' has been shown to negatively impact male reproduction. This study revealed for the first time that IVM induces apoptosis in mouse spermatogonia via ER and mitochondrial dysfunction driven by ROS accumulation, Ca2+ overload, and protein misfolding. To an extent, Se was found to counteract these effects through the activation of selenoprotein-encoding genes such as *Gpx4* and *Selenov*. These findings suggest that Se is a valuable protective agent against oxidative and ER stress to preserve male fertility.

CRediT authorship contribution statement

Sung-Hwan Moon: Writing – review & editing, Methodology. **Buom-Yong Ryu:** Writing – review & editing, Validation, Supervision, Resources, Project administration, Funding acquisition. **Daniel Chavez Varias:** Writing – review & editing, Writing – original draft, Visualization, Methodology, Investigation, Formal analysis, Data curation, Conceptualization. **Seung Hee Shin:** Writing – review & editing, Methodology.

Declaration of Competing Interest

The authors declare that they have no known competing financial interests or personal relationships that could have appeared to influence the work reported in this paper.

Acknowledgements

The Basic Science Research Program through the National Research Foundation of Korea (NRF), funded by the Ministry of Education (NRF2018R1A6A1A03025159) supported this work. Also, this research was supported by the Chung-Ang University Young Scientist Scholarship in 2023. We thank J. Kim of the BT Research Facility Center, Chung-Ang University for their technical assistance.

Appendix A. Supporting information

Supplementary data associated with this article can be found in the online version at doi:10.1016/j.ecoenv.2024.117307.

Data availability

Data will be made available on request.

References

Abo El-Magd, N.F., Barbosa, P.O., Nick, J., Covalero, V., Grignetti, G., Bermano, G., 2022. Selenium, as selenite, prevents adipogenesis by modulating selenoproteins gene expression and oxidative stress–related genes. Nutrition 93, 111424. https://doi.org/10.1016/j.nut.2021.111424.

Ahmed, A.E., Alshehri, A., Al-Kahtani, M.A., Elbehairi, S.E.I., Alshehri, M.A., Shati, A.A., Alfaifi, M.Y., Al-Doais, A.A., Taha, R., Morsy, K., El-Mansi, A.A., 2020. Vitamin E and selenium administration synergistically mitigates ivermectin and doramectin-induced testicular dysfunction in male Wistar albino rats. Biomed. Pharmacother. 124, 109841. https://doi.org/10.1016/j.biopha.2020.109841.

AlOkda, A., Van Raamsdonk, J.M., 2023. Evolutionarily conserved role of thioredoxin systems in determining longevity. Antioxidants 12. https://doi.org/10.3390/antiox12040944.

Atif, M., Smith, J.J., Estrada-Mondragon, A., Xiao, X., Salim, A.A., Capon, R.J., Lynch, J. W., Keramidas, A., 2019. GluClR-mediated inhibitory postsynaptic currents reveal targets for ivermectin and potential mechanisms of ivermectin resistance. PLOS Pathog. 15, e1007570. https://doi.org/10.1371/journal.ppat.1007570.

Bai, S.H., Ogbourne, S., 2016. Eco-toxicological effects of the avermectin family with a focus on abamectin and ivermectin. Chemosphere 154, 204–214. https://doi.org/10.1016/j.chemosphere.2016.03.113.

Beriault, D.R., Werstuck, G.H., 2013. Detection and quantification of endoplasmic reticulum stress in living cells using the fluorescent compound, Thioflavin T. Biochim. Et. Biophys. Acta (BBA) - Mol. Cell Res. 1833, 2293–2301. https://doi.org/10.1016/j.bbamcr.2013.05.020.

Bhattarai, K.R., Riaz, T.A., Kim, H.-R., Chae, H.-J., 2021. The aftermath of the interplay between the endoplasmic reticulum stress response and redox signaling. Exp. Mol. Med. 53, 151–167. https://doi.org/10.1038/s12276-021-00560-8.

Boussinesq, M., 2018. A new powerful drug to combat river blindness. Lancet 392, 1170–1172. https://doi.org/10.1016/S0140-6736(18)30101-6.

Brigelius-Flohé, R., Maiorino, M., 2013. Glutathione peroxidases. Biochim. Et. Biophys. Acta (BBA) - Gen. Subj. 1830, 3289–3303. https://doi.org/10.1016/j.bbagen.2012.11.020.

Byun, B.J., Kang, Y.K., 2011. Conformational preferences and pKa value of selenocysteine residue. Biopolymers 95, 345–353. https://doi.org/10.1002/bip.21581.

Cao, S.S., Kaufman, R.J., 2014. Endoplasmic reticulum stress and oxidative stress in cell fate decision and human disease. Antioxid. Redox Signal 21, 396–413. https://doi.org/10.1089/ars.2014.5851.

Cao, W., Zhao, M., Chen, Y., Zhu, J., Xie, C., Li, X., Geng, S., Zhong, C., Fu, J., Wu, J., 2023. Low-dose phthalates promote breast cancer stem cell properties via the oncogene ΔNp63α and the Sonic hedgehog pathway. Ecotoxicol. Environ. Saf. 252, 114605. https://doi.org/10.1016/j.ecoenv.2023.114605.

Chaccour, C., Rabinovich, N.R., 2019. Advancing the repurposing of ivermectin for malaria. Lancet 393, 1480–1481. https://doi.org/10.1016/S0140-6736(18)32613-8.

Chen, L., Bi, S., Wei, Q., Zhao, Z., Wang, C., Xie, S., 2020. Ivermectin suppresses tumour growth and metastasis through degradation of PAK1 in oesophageal squamous cell carcinoma. J. Cell Mol. Med. 24, 5387–5401. https://doi.org/10.1111/jcmm.15195.

Chen, L.-L., Huang, J.-Q., Wu, Y.-Y., Chen, L.-B., Li, S.-P., Zhang, X., Wu, S., Ren, F.-Z., Lei, X.-G., 2021. Loss of Selenov predisposes mice to extra fat accumulation and attenuated energy expenditure. Redox Biol. 45, 102048. https://doi.org/10.1016/j.redox.2021.102048.

Chen, L., Na, R., Danae McLane, K., Thompson, C.S., Gao, J., Wang, X., Ran, Q., 2021. Overexpression of ferroptosis defense enzyme Gpx4 retards motor neuron disease of SOD1G93A mice. Sci. Rep. 11, 12890. https://doi.org/10.1038/s41598-021-92369-8.

Chipurupalli, S., Samavedam, U., Robinson, N., 2021. Crosstalk between ER stress, autophagy and inflammation. Front. Med. 8.

Choudhury, A., Das, N.C., Patra, R., Bhattacharya, M., Ghosh, P., Patra, B.C., Mukherjee, S., 2021. Exploring the binding efficacy of ivermectin against the key proteins of SARS-CoV-2 pathogenesis: an *in silico* approach. Future Virol. 16, 277–291. https://doi.org/10.2217/fvl-2020-0342.

Cordeiro, F., Gonçalves, V., Moreira, N., Slobodticov, J.I., de Andrade Galvão, N., de Souza Spinosa, H., Bonamin, L.V., Bondan, E.F., Ciscato, C.H.P., Barbosa, C.M., Bernardi, M.M., 2018. Ivermectin acute administration impaired the spermatogenesis and spermiogenesis of adult rats. Res. Vet. Sci. 117, 178–186. https://doi.org/10.1016/j.rvsc.2017.12.013.

Ding, D., Mou, D., Zhu, H., Jiang, X., Che, L., Fang, Z., Xu, S., Lin, Y., Zhuo, Y., Li, J., Huang, C., Zou, Y., Li, L., Wu, D., Feng, B., 2022. Maternal organic selenium supplementation relieves intestinal endoplasmic reticulum stress in piglets by enhancing the expression of glutathione peroxidase 4 and selenoprotein S. Front. Nutr. 9.

Dou, Q., Chen, H.-N., Wang, K., Yuan, K., Lei, Y., Li, K., Lan, J., Chen, Y., Huang, Z., Xie, N., Zhang, L., Xiang, R., Nice, E.C., Wei, Y., Huang, C., 2016. Ivermectin induces cytostatic autophagy by blocking the PAK1/Akt axis in breast cancer. Cancer Res. 76, 4457–4469. https://doi.org/10.1158/0008-5472.CAN-15-2887.

Draganov, D., Han, Z., Rana, A., Bennett, N., Irvine, D.J., Lee, P.P., 2021. Ivermectin converts cold tumors hot and synergizes with immune checkpoint blockade for treatment of breast cancer. npj Breast Cancer 7, 1–11. https://doi.org/10.1038/s41523-021-00229-5.

EL-Maddawy, Z.K., Abd El Naby, W.S.H., 2018. Effects of ivermectin and its combination with alpha lipoic acid on expression of IGFBP-3 and HSPA1 genes and male rat fertility. Andrologia 50, e12891. https://doi.org/10.1111/and.12891.

El-Nahas, A.F., El-Ashmawy, I.M., 2008. Effect of ivermectin on male fertility and its interaction with P-glycoprotein inhibitor (verapamil) in rats. Environ. Toxicol. Pharmacol. 26, 206–211. https://doi.org/10.1016/j.etap.2008.03.011.

El-Shobokshy, S.A., Abo-Samaha, M.I., Sahwan, F.M., El-Rheem, S.M.A., Emam, M., Khafaga, A.F., 2023. Implication of apoptosis and oxidative stress in mitigation of ivermectin long-term hazards by zinc nanoparticles in male rabbits. Environ. Sci. Pollut. Res. 30, 26982–26997. https://doi.org/10.1007/s11356-022-24095-1.

European Food Safety Authority (EFSA), Alvarez, F., Arena, M., Auteri, D., Binaglia, M., Castoldi, A.F., Chiusolo, A., Colagiorgi, A., Colas, M., Crivellente, F., De Lentdecker, C., Egsmose, M., Fait, G., Ferilli, F., Gouliarmou, V., Nogareda, L.H., Ippolito, A., Istace, F., Jarrah, S., Kardassi, D., Kienzler, A., Lanzoni, A., Lava, R., Leuschner, R., Linguadoca, A., Lythgo, C., Magrans, O., Mangas, I., Miron, I., Molnar, T., Padovani, L., Parra Morte, J.M., Serafimova, R., Sharp, R., Szentes, C., Terron, A., Theobald, A., Tiramani, M., Villamar-Bouza, L., 2022. Peer review of the pesticide risk assessment of the active substance abamectin. EFSA J. 20, e07544. https://doi.org/10.2903/j.efsa.2022.7544.

Foy, B.D., Alout, H., Seaman, J.A., Rao, S., Magalhaes, T., Wade, M., Parikh, S., Soma, D. D., Sagna, A.B., Fournet, F., Slater, H.C., Bougma, R., Drabo, F., Diabaté, A., Coulidiaty, A.G.V., Rouamba, N., Dabiré, R.K., 2019. Efficacy and risk of harms of repeat ivermectin mass drug administrations for control of malaria (RIMDAMAL): a cluster-randomised trial. Lancet 393, 1517–1526. https://doi.org/10.1016/S0140-6736(18)32321-3.

Gan, J., Ji, X., Jin, X., Zhou, M., Yang, C., Chen, Z., Yin, C., Dong, Z., 2024. Silybin protected from avermectin-induced carp (Cyprinus carpio) nephrotoxicity by regulating PPAR-γ-involved inflammation, oxidative stress, ferroptosis and autophagy. Aquat. Toxicol. 273, 107011. https://doi.org/10.1016/j.aquatox.2024.107011.

Gouveia, A., Bajwa, E., Klegeris, A., 2017. Extracellular cytochrome c as an intercellular signaling molecule regulating microglial functions. Biochim. Et. Biophys. Acta (BBA) - Gen. Subj. 1861, 2274–2281. https://doi.org/10.1016/j.bbagen.2017.06.017.

Hetz, C., 2012. The unfolded protein response: controlling cell fate decisions under ER stress and beyond. Nat. Rev. Mol. Cell Biol. 13, 89–102. https://doi.org/10.1038/nrm3270.

Ho, D.V., Chan, J.Y., 2015. Induction of Herpud1 expression by ER stress is regulated by Nrf1. FEBS Lett. 589, 615–620. https://doi.org/10.1016/j.febslet.2015.01.026.

Huang, Y., Hong, Y., Huang, Z., Zhang, J., Huang, Q., 2019. Avermectin induces the oxidative stress, genotoxicity, and immunological responses in the Chinese Mitten Crab, Eriocheir sinensis. PLOS ONE 14, e0225171. https://doi.org/10.1371/journal.pone.0225171.

Javid, J., Mir, R., Julka, P.K., Ray, P.C., Saxena, A., 2015. Extracellular cytochrome c as a biomarker for monitoring therapeutic efficacy and prognosis of non-small cell lung cancer patients. Tumor Biol. 36, 4253–4260. https://doi.org/10.1007/s13277-015-3062-6.

Jawad, M.J., Richardson, A., 2023. Ivermectin augments the anti-cancer activity of pitavastatin in ovarian cancer cells. Diseases 11, 49. https://doi.org/10.3390/diseases11010049.

Kim, S.G., Jeon, J.H., Shin, S.H., Varias, D.C., Moon, S.-H., Ryu, B.-Y., 2024. Inhibition of reactive oxygen species generation by N-Acetyl Cysteine can mitigate male germ cell toxicity induced by bisphenol analogs. Food Chem. Toxicol. 188, 114652. https://doi.org/10.1016/j.fct.2024.114652.

Laman, M., Tavul, L., Karl, S., Kotty, B., Kerry, Z., Kumai, S., Samuel, A., Lorry, L., Timinao, L., Howard, S.C., Makita, L., John, L., Bieb, S., Wangi, J., Albert, J.M., Payne, M., Weil, G.J., Tisch, D.J., Bjerum, C.M., Robinson, L.J., King, C.L., 2022. Mass drug administration of ivermectin, diethylcarbamazine, plus albendazole compared with diethylcarbamazine plus albendazole for reduction of lymphatic filariasis endemicity in Papua New Guinea: a cluster-randomised trial. Lancet Infect. Dis. 22, 1200–1209. https://doi.org/10.1016/S1473-3099(22)00026-3.

Lee, B.W.L., Ghode, P., Ong, D.S.T., 2019. Redox regulation of cell state and fate. Redox Biol., Redox Regul. Cell State Fate 25, 101056. https://doi.org/10.1016/j.redox.2018.11.014.

Lee, D.E., Kang, H.W., Kim, S.Y., Kim, M.J., Jeong, J.W., Hong, W.C., Fang, S., Kim, H.S., Lee, Y.S., Kim, H.J., Park, J.S., 2022. Ivermectin and gemcitabine combination treatment induces apoptosis of pancreatic cancer cells via mitochondrial dysfunction. Front Pharm. 13, 934746. https://doi.org/10.3389/fphar.2022.934746.

Lee, R., Kim, D.-W., Lee, W.-Y., Park, H.-J., 2022. Zearalenone induces apoptosis and autophagy in a spermatogonia cell line. Toxins 14. https://doi.org/10.3390/toxins14020148.

Lei, B., Sun, S., Zhang, X., Feng, C., Xu, J., Wen, Y., Huang, Y., Wu, M., Yu, Y., 2019. Bisphenol AF exerts estrogenic activity in MCF-7 cells through activation of Erk and PI3K/Akt signals via GPER signaling pathway. Chemosphere 220, 362–370. https://doi.org/10.1016/j.chemosphere.2018.12.122.

Li, J., Qi, F., Su, H., Zhang, C., Zhang, Q., Chen, Ying, Chen, P., Su, L., Chen, Yanan, Yang, Y., Chen, Z., Zhang, S., 2022. GRP75-faciliated mitochondria-associated ER membrane (MAM) integrity controls cisplatin-resistance in ovarian cancer patients. Int J. Biol. Sci. 18, 2914–2931. https://doi.org/10.7150/ijbs.71571.

Liu, A., Li, F., Xu, P., Chen, Y., Liang, X., Zheng, S., Meng, H., Zhu, Y., Mo, J., Gong, C., Zhou, J.-C., 2023. Gpx4, Selenov, and Txnrd3 are three most testis-abundant selenogenes resistant to dietary selenium concentrations and actively expressed during reproductive ages in rats. Biol. Trace Elem. Res 201, 250–259. https://doi.org/10.1007/s12011-022-03118-5.

Liu, M., Shi, X., Bi, Y., Qi, L., Guo, X., Wang, L., Zhou, Z., Sha, J., 2014. SHCBP1L, a conserved protein in mammals, is predominantly expressed in male germ cells and maintains spindle stability during meiosis in testis. Mol. Hum. Reprod. 20, 463–475. https://doi.org/10.1093/molehr/gau014.

Ma, L., Hai, S., Wang, C., Chen, C., Rahman, S.U., Zhao, C., Bazai, M.A., Feng, S., Wang, X., 2023. Zearalenone induces mitochondria-associated endoplasmic reticulum membranes dysfunction in piglet Sertoli cells based on endoplasmic reticulum stress. Ecotoxicol. Environ. Saf. 254, 114710. https://doi.org/10.1016/j.ecoenv.2023.114710.

Mesa, L., Gutiérrez, Ma.F., Montalto, L., Perez, V., Lifschitz, A., 2020. Concentration and environmental fate of ivermectin in floodplain wetlands: an ecosystem approach. Sci. Total Environ. 706, 135692. https://doi.org/10.1016/j.scitotenv.2019.135692.

Nagai, H., Satomi, T., Abiru, A., Miyamoto, K., Nagasawa, K., Maruyama, M., Yamamoto, S., Kikuchi, K., Fuse, H., Noda, M., Tsujihata, Y., 2017. Antihypertrophic effects of small molecules that maintain mitochondrial atp levels under hypoxia. eBioMedicine 24, 147–158. https://doi.org/10.1016/j.ebiom.2017.09.022.

Nancharaiah, Y.V., Lens, P.N.L., 2015. Ecology and biotechnology of selenium-respiring bacteria. Microbiol. Mol. Biol. Rev. 79, 61–80. https://doi.org/10.1128/mmbr.00037-14.

Novelli, A., Vieira, B.H., Braun, A.S., Mendes, L.B., Daam, M.A., Espíndola, E.L.G., 2016. Impact of runoff water from an experimental agricultural field applied with Vertimec® 18EC (abamectin) on the survival, growth and gill morphology of zebrafish juveniles. Chemosphere 144, 1408–1414. https://doi.org/10.1016/j.chemosphere.2015.10.004.

Oslowski, C.M., Urano, F., 2011. Measuring ER stress and the unfolded protein response using mammalian tissue culture system. Methods Enzym. 490, 71–92. https://doi.org/10.1016/B978-0-12-385114-7.00004-0.

Pitts, M.W., Hoffmann, P.R., 2018. Endoplasmic reticulum-resident selenoproteins as regulators of calcium signaling and homeostasis. Cell Calcium, role Ca2+ Signals Regul. Cell death Surviv. Process. Health, Dis. Ther. 70, 76–86. https://doi.org/10.1016/j.ceca.2017.05.001.

Reeves, M.A., Bellinger, F.P., Berry, M.J., 2010. The neuroprotective functions of selenoprotein m and its role in cytosolic calcium regulation. Antioxid. Redox Signal. 12, 809–818. https://doi.org/10.1089/ars.2009.2883.

Renz, A., Berdel, W.E., Kreuter, M., Belka, C., Schulze-Osthoff, K., Los, M., 2001. Rapid extracellular release of cytochrome c is specific for apoptosis and marks cell death in vivo. Blood 98, 1542–1548. https://doi.org/10.1182/blood.V98.5.1542.

Salman, M., Abbas, R.Z., Mehmood, K., Hussain, R., Shah, S., Faheem, M., Zaheer, T., Abbas, A., Morales, B., Aneva, I., Martínez, J.L., 2022. Assessment of avermectins-induced toxicity in animals. Pharmaceuticals 15. https://doi.org/10.3390/ph15030332.

Schmith, V.D., Zhou, J. (Jessie), Lohmer, L.R.L., 2020. The approved dose of ivermectin alone is not the ideal dose for the treatment of COVID-19. Clin. Pharmacol. Ther. 108, 762–765. https://doi.org/10.1002/cpt.1889.

Shin, E.M., Hay, H.S., Lee, M.H., Goh, J.N., Tan, T.Z., Sen, Y.P., Lim, S.W., Yousef, E.M., Ong, H.T., Thike, A.A., Kong, X., Wu, Z., Mendoz, E., Sun, W., Salto-Tellez, M., Lim, C.T., Lobie, P.E., Lim, Y.P., Yap, C.T., Zeng, Q., Sethi, G., Lee, M.B., Tan, P., Goh, B.C., Miller, L.D., Thiery, J.P., Zhu, T., Gaboury, L., Tan, P.H., Hui, K.M., Yip, G. W.-C., Miyamoto, S., Kumar, A.P., Tergaonkar, V., 2014. DEAD-box helicase DP103 defines metastatic potential of human breast cancers. J. Clin. Invest 124, 3807–3824. https://doi.org/10.1172/JCI73451.

Specht, S., Keiser, J., 2023. Helminth infections: enabling the world health organization road map. Int. J. Parasitol., Anthelmintics V: Drugs, Resist., Vaccin. 53, 411–414. https://doi.org/10.1016/j.ijpara.2022.10.006.

Sulik, M., Antoszczak, M., Huczyński, A., Steverding, D., 2023. Antiparasitic activity of ivermectin: four decades of research into a “wonder drug”. Eur. J. Med. Chem. 261, 115838. https://doi.org/10.1016/j.ejmech.2023.115838.

Tiwary, S., Nandwani, A., Khan, R., Datta, M., 2021. GRP75 mediates endoplasmic reticulum–mitochondria coupling during palmitate-induced pancreatic β-cell apoptosis. J. Biol. Chem. 297, 101368. https://doi.org/10.1016/j.jbc.2021.101368.

Tsheten, T., Alene, K.A., Restrepo, A.C., Kelly, M., Lau, C., Clements, A.C.A., Gray, D.J., Daga, C., Mapalo, V.J., Espino, F.E., Wangdi, K., 2024. Risk mapping and socio-ecological drivers of soil-transmitted helminth infections in the Philippines: a spatial modelling study. Lancet Reg. Health – West. Pac. 43. https://doi.org/10.1016/j.lanwpc.2023.100974.

Tung, C.-L., Chao, W.-Y., Li, Y.-Z., Shen, C.-H., Zhao, P.-W., Chen, S.-H., Wu, T.-Y., Lee, Y.-R., 2022. Ivermectin induces cell cycle arrest and caspase-dependent apoptosis in human urothelial carcinoma cells. Int J. Med Sci. 19, 1567–1575. https://doi.org/10.7150/ijms.76623.

Vandenberg, L.N., Colborn, T., Hayes, T.B., Heindel, J.J., Jacobs Jr., D.R., Lee, D.-H., Shioda, T., Soto, A.M., vom Saal, F.S., Welshons, W.V., Zoeller, R.T., Myers, J.P., 2012. Hormones and endocrine-disrupting chemicals: low-dose effects and nonmonotonic dose responses. Endocr. Rev. 33, 378–455. https://doi.org/10.1210/er.2011-1050.

Varlamova, E.G., Goltyaev, M.V., Turovsky, E.A., 2022. The role of selenoproteins SELENOM and SELENOT in the regulation of apoptosis, ER stress, and calcium homeostasis in the A-172 human glioblastoma cell line. Biology 11. https://doi.org/10.3390/biology11060811.

Whelan, E.C., Yang, F., Avarbock, M.R., Sullivan, M.C., Beiting, D.P., Brinster, R.L., 2022. Reestablishment of spermatogenesis after more than 20 years of cryopreservation of rat spermatogonial stem cells reveals an important impact in differentiation capacity. PLOS Biol. 20, e3001618. https://doi.org/10.1371/journal.pbio.3001618.

Xu, C., Cao, Y., Bao, J., 2021. Building RNA-protein germ granules: insights from the multifaceted functions of DEAD-box helicase Vasa/Ddx4 in germline development. Cell. Mol. Life Sci. 79, 4. https://doi.org/10.1007/s00018-021-04069-1.

Xu, N., Lu, M., Wang, J., Li, Yujia, Yang, X., Wei, X., Si, J., Han, J., Yao, X., Zhang, J., Liu, J., Li, Yanming, Yang, H., Bao, D., 2021. Ivermectin induces apoptosis of esophageal squamous cell carcinoma via mitochondrial pathway. BMC Cancer 21, 1307. https://doi.org/10.1186/s12885-021-09021-x.

Ye, R., Huang, J., Wang, Z., Chen, Y., Dong, Y., 2021. Trace element selenium effectively alleviates intestinal diseases. Int. J. Mol. Sci. 22. https://doi.org/10.3390/ijms222111708.

Zhang, Y., Li, G., Zhao, Y., Dai, X., Hu, M., Cao, H., Huang, K., Yang, F., 2023. Inhibition of calcium imbalance protects hepatocytes from vanadium exposure-induced inflammation by mediating mitochondrial-associated endoplasmic reticulum membranes in ducks. Poult. Sci. 102, 103013. https://doi.org/10.1016/j.psj.2023.103013.

Zhang, T., Sun, S., Gavrilović, A., Li, D., Tang, R., 2023. Selenium alleviates cadmium-induced oxidative stress, endoplasmic reticulum stress, and apoptosis in L8824 cells. Ecotoxicol. Environ. Saf. 262, 115337. https://doi.org/10.1016/j.ecoenv.2023.115337.

Zhang, Y., Sun, T., Li, M., Lin, Y., Liu, Y., Tang, S., Dai, C., 2022. Ivermectin-induced apoptotic cell death in human SH-SY5Y cells involves the activation of oxidative stress and mitochondrial pathway and Akt/mTOR-pathway-mediated autophagy. Antioxidants 11, 908. https://doi.org/10.3390/antiox11050908.

Zhang, X., Xiong, W., Chen, L.-L., Huang, J.-Q., Lei, X.G., 2020. Selenoprotein V protects against endoplasmic reticulum stress and oxidative injury induced by pro-oxidants. Free Radic. Biol. Med. 160, 670–679. https://doi.org/10.1016/j.freeradbiomed.2020.08.011.

Zhang, Y., Yang, A., Zhao, Z., Chen, F., Yan, X., Han, Y., Wu, D., Wu, Y., 2024. Protein disulfide isomerase is essential for spermatogenesis in mice. JCI Insight 9. https://doi.org/10.1172/jci.insight.177743.

Zhang, P., Zhang, Y., Liu, K., Liu, B., Xu, W., Gao, J., Ding, L., Tao, L., 2019. Ivermectin induces cell cycle arrest and apoptosis of HeLa cells via mitochondrial pathway. Cell Prolif. 52, e12543. https://doi.org/10.1111/cpr.12543.

Zhang, Z., Zhang, L., Zhou, L., Lei, Y., Zhang, Y., Huang, C., 2019. Redox signaling and unfolded protein response coordinate cell fate decisions under ER stress. Redox Biol. 25, 101047. https://doi.org/10.1016/j.redox.2018.11.005.

Zhu, M., Li, Y., Zhou, Z., 2017. Antibiotic ivermectin preferentially targets renal cancer through inducing mitochondrial dysfunction and oxidative damage. Biochem. Biophys. Res. Commun. 492, 373–378. https://doi.org/10.1016/j.bbrc.2017.08.097.

Zoidis, E., Seremelis, I., Kontopoulos, N., Danezis, G.P., 2018. Selenium-dependent antioxidant enzymes: actions and properties of selenoproteins. Antioxidants 7, 66. https://doi.org/10.3390/antiox7050066.